PAPER

Check for updates

In situ reduction of chloroauric acid (HAuCl$_4$) for generation of catalytic Au nanoparticle embedded triazine based covalent organic polymer networks

Sami Dursun, [iD] *[ab] Emine Yavuz [iD] *[b] and Zeynep Çetinkaya [iD] [ab]

Covalent-organic polymer networks (COPNs) have been used as catalyst supports due to their stable and favorable structure. Herein, a simple synthetic route was applied to generate Au@COPN-1 hybrids *via in situ* reduction of gold ions with no additional reducing agent. Synthesized novel COPN-1 was mixed with different concentrations of HAuCl$_4$ which resulted in Au@COPN-1 with varying sizes of Au nanoparticles in a controlled manner. The microstructural and morphological features of COPN-1 and Au@COPN-1 were characterized in detail using FT-IR, C-NMR, elemental analysis, UV-Vis, XRD, TEM, BET, and TGA. It is noteworthy that the red-shifted LSPR peaks of Au nanoparticles produced with increasing concentrations of HAuCl$_4$ indicated an increase in the particle size of the Au nanoparticles as justified by TEM images. The optimum catalytic activity of Au@COPN-1 was obtained when 4.6×10^{-3} mM HAuCl$_4$ was used, which led to the complete reduction of 4-nitrophenol within 16 minutes with excellent recyclability for more than 5 catalytic cycles, giving yields over 94%. Moreover, the non-aggregation of nanoparticles in the reused catalyst further confirmed the stability of the prepared catalysts. Consequently, these results indicated that *in situ* synthesis of AuNPs inside the COPN-1 matrix produces a promising catalyst platform for the reduction of aromatic nitro compounds, for example, for the degradation of one of the most common persistent organic pollutants 4-nitrophenol, as shown here. In addition, the Au@COPN-1 hybrid system showed good biocompatibility at appropriate doses confirmed by a dynamic real-time cell analysis system which can be used in various medical applications, such as drug delivery, in the future.

1. Introduction

Metal nanoparticles have gained great attention due to their outstanding properties and applications. In particular, gold nanoparticles (AuNPs) have unique characteristics such as inertness, tunable localized surface plasmon resonance, and easy surface modification which enable various applications especially in the field of drug delivery, catalysis, optical devices, biosensors, and nanofabrication.[1–6] In heterogeneous catalysis, because of having high surface-to-volume ratios, small AuNPs possess unique analytical activities in hydrogenation, C–C coupling, and oxidation reactions with high conversion rates even at low temperatures.[7–10] However, the aggregation tendency of AuNPs limits their usage in catalyst systems, particularly at the industrial scale. Therefore, the immobilization of AuNPs on solid supports has been attracted great attention as one of the best promising strategies to overcome aggregation hurdle.[11,12]

Among the suitable solid supports, the porous materials such as zeolites, activated carbon, dendrimers, and polymer networks have been widely used due to their high surface areas and large pore volumes.[13–15] Recently, the usage of covalent-organic polymer networks (COPN) has been exploited as catalyst support owing to chemical tailoring of its network surface, well-defined porosity, and chemically stable covalent bonded structure.[16–18] For instance, highly stable and porous COF synthesized by the Mannich-coupling reaction was used to generate robust Au(0)@TpPa-1 *via* the reduction of adsorbed HAuCl$_4$ in the presence of NaBH$_4$, a strong reducing agent.[19] This Au(0)-based catalyst system showed a good catalytic activity towards the reduction of anthropogenic and toxic chemical, 4-nitrophenol. The synthetic protocols excluding the usage of any additional chemical reagents (*i.e.* surfactant, a reducing agent or solvent), which may be difficult to eliminate from the catalysis platform, subsequently are very beneficial for practical applications, especially in biocatalysis.[20–22]

The *in situ* reduction of Au(+3) ions adsorbed onto a porous material, without using any reducing agent, is a superior technique to generate Au(0) catalysis system with fewer production steps which makes the elimination of any

[a]Department of Metallurgical and Materials Engineering, Konya Technical University, Konya, Turkey. E-mail: samidursun@ktun.edu.tr; Tel: +90 332 223 2238

[b]Advanced Technology Research and Application Center, Selcuk University, Konya, Turkey. E-mail: emineyavuz@selcuk.edu.tr; Tel: +90 332 223 0742

contamination caused by the reducing agent possible. The *in situ* approach offers significant assets including the stabilization of AuNPs inside the porous matrix, generation of small catalytic AuNPs, the formation of AuNPs species only inside the porous material, and prevention of nanoparticle aggregation. As an example, Au(+3) ions adsorbed onto porous chitosan beads and films were reduced *in situ* by chitosan.[23,24] In addition, the reduction of $HAuCl_4$ with chitosan itself induced chitosan gelation to form AuNP@chitosan scaffolds.[25] In other study, AuNPs embedded polydimethylsiloxane (PDMS) composite films were successfully prepared by reducing $HAuCl_4$ with Si–H functional unit inside the PDMS.[26] In another study, Au nanoparticle decorated polypyrrole (PPy) nanotubes by *in situ* reduction process was presented. Au nanoparticles are stored by reducing $HAuCl_4$ in PPy nanotubes.[27]

Herein, we reported a simple synthetic route to generate Au@COPN-1 hybrids *via in situ* reduction of gold ions Au(+3) without using an extra-reducing agent. COPN-1, synthesized by epoxy-amine coupling reaction, was mixed with $HAuCl_4$ and resulted in Au@COPN-1 due to the reduction of adsorbed Au(+3) with free alcohol (OH) units of COPN-1 formed during an epoxy-amine reaction. COPN-1 and Au@COPN-1 were spectroscopically characterized. Besides the effect of different $HAuCl_4$ concentrations on the final product Au@COPN-1, the catalytic activities of this hybrid material towards 4-nitrophenol reduction were also investigated. Moreover, the biocompatibility of Au@COPN-1 was investigated in L929 cells which confirmed its possible usage in bioapplications.

2. Experimental

2.1. Chemicals

Tris(2,3-epoxypropyl)isocyanurate (TEPIC), melamine (99%), tetraethylene glycol dimethyl ether (TEGDME, 99%), gold(III) chloride trihydrate ACS reagent(≥49.0%, $HAuCl_4 \cdot 3H_2O$), 4-nitrophenol (99%, 4-Nph) and sodium borohydride (≥98.0%, $NaBH_4$) were purchased from Sigma Aldrich. Acetone (ACS, ISO, Reag. PhEur) was obtained from Merck Chemical Company. All chemicals were used as received without any further purification. The water used in all experiments was deionized water with a resistivity of 18 MW cm^{-1}, which was prepared by an ultrapure water system (Aqua Solutions).

2.2. Synthesis of porous covalent organic polymer (COPN-1)

Melamine (0.4255 g, 3.3647 mmol) was dissolved in tetraethylene glycol dimethyl ether(4 mL) at 165 °C and tris(2,3-epoxypropyl)isocyanurate (1 g, 3.3647 mmol) was dissolved in tetraethylene glycol dimethyl ether (4 mL) at 70 °C, separately. Then, tris(2,3-epoxypropyl)isocyanurate solution was added dropwise to the 250 mL flask containing melamine solution under continuous stirring at 165 °C. After 3 hours, the brown precipitate was obtained and this precipitate was washed thrice with acetone (15 mL), then thrice with distilled water (15 mL). The light brown solid product (COPN-1) was dried by using a vacuum oven at 75 °C for 3 hours.

2.3. Synthesis of porous covalent organic polymer with gold(III) chloride trihydrate (Au@COPN-1)

As-synthesized COPN-1 (100 mg) was soaked in distilled water (5 mL). Then, gold(III) chloride trihydrate (10 mg, 0.0254 mmol) in 1 mL distilled water solution was added dropwise to the COPN-1 solution under continuous stirring. The mixture was stirred at room temperature for 12 hours. Afterward, the flask containing $HAuCl_4 \cdot 3H_2O$ and COPN-1 mixture was inserted into an oil bath at 100 °C. After heating 3 hours, the mixture was cooled to room temperature. The solid crude was washed thrice with distilled water and then dried with a vacuum oven at 75 °C for 3 hours to yield a dark red solid product.

2.4. Catalytic activity measurement

Stock solutions of 16 mg $NaBH_4$ in 10 mL distilled water and 10 mg 4-nitrophenol in 50 mL distilled water were prepared at room temperature. 1 mL of each solution was taken and transferred to a 5 mL vial under stirring. Following the addition of 50 mg Au@COPN-1 (9.2×10^{-3} mM Au) to the vial, the catalysis reaction was started. UV-Vis spectra were recorded at every two-second within the range of 250–550 nm to monitor the catalysis reaction.

2.5. Recyclability test of 4-nitrophenol

After the first run reaction was completed, the residual solid was recovered by filtration. Then, the residual solid was washed with distilled water, methanol and dichloromethane and then dried in air. The catalyst was dried in air and was used for the next run with the same amount of fresh 4-nitrophenol and $NaBH_4$.

2.6. Real-time analysis of cell proliferation

L929 cells, an immortal non-cancerous mouse fibroblast cell line frequently used in cytotoxicity screening tests, were cultured in DMEM media supplemented with high glucose, L-glutamine, sodium pyruvate, 1% penicillin/streptomycin, and 10% heated-inactivated FBS in a humidified incubator of 5% CO_2 at 37 °C. Cell proliferation was monitored by the impedance-based xCELLigence real-time cell analyzer dual plate instrument (RTCA DP, ACEA Biosciences, San Diego, CA) according to manufacturer's instructions. Briefly, background measurement was performed first. Then L929 cells were seeded (1×10^4 cells per well) into the E-plate 16 (ACEA Biosciences, San Diego, CA, USA) with a volume of 100 μl and allowed to attach before treatment. The cell index (CI) values were monitored automatically every 1 h at 37 °C in a 5% CO_2 atmosphere. When the cells entered the log phase, Au@COPN-1 was added at concentrations of 500, 250, 125, and 62.5 μg mL^{-1} and impedance was measured every 15 min for at least 250 h. Control groups were treated with medium only. The measurements were analyzed by normalizing data of every single well to the first measurement after adding Au@COPN-1 as the normalized cell index. The RTCA software v. 2.0.0 was used to obtain viability profiles of the cells treated with different concentrations of Au@COPN-1 and the cytotoxic effect of Au@COPN-1 was quantified by calculating the half-maximal inhibitory concentration (IC_{50}).

2.7. Characterization

FTIR spectrum of the COPN-1 was recorded over the range of 4000–500 cm^{-1} at a resolution of 4 cm^{-1} using FTIR spectroscopy (VERTEX-70 Bruker, Germany). Elemental analysis was performed using a PerkinElmer 2400 CHN elemental analyzer. Solid-state ^{13}C CP/MAS NMR was recorded on a Bruker SB Avance III 500 MHz spectrometer with a 4 mm double-resonance MAS probe, a sample spinning rate of 8.0 kHz, a contact time of 2 ms and a pulse delay of 5 s. To evaluate the porosity of COPN-1, adsorption isotherms were obtained with a Micromeritics Tristar II 3020 accelerated surface area and porosimetry analyzer at 77 K, after the samples were degassed at 75 °C for 6 h under vacuum. The adsorption–desorption isotherms were obtained to give the BET ($P/P_o = 0.01$–0.25) and Langmuir ($P/P_o = 0.1$–0.35) surface area. The UV-Vis spectra from 400–700 nm were recorded using a Biochrom Libra S22 spectrometer using quartz cuvettes. X-ray diffraction (XRD) analyses were performed for phase identification of the products. A BRUKER D8 ADVANCE diffractometer was used, using Cu-Kα radiation ($\lambda = 1.54$ Å) and X-ray source operating voltage of 40 kV in the 2θ range of 10–75° at a scanning rate of 2° min^{-1}. To prepare samples for TEM, a drop of the nanoparticle suspension (in water) was placed on a carbon-coated copper grid and dried under ambient conditions in the fume hood. High-resolution TEM images were taken using a JEOL 2100F microscope operated at 200 kV. TGA analysis of the samples was performed on Mettler Toledo analyzer under N$_2$ and air atmosphere at a heating rate of 10 °C min^{-1} within a temperature range of 25–800 °C.

3. Results and discussion

Covalent organic polymer networks (COPN-1) shown in Scheme 1 was prepared by reacting melamine with tris(2,3-epoxypropyl) isocyanurate (TEPIC) at high temperature *via* the Mannich-coupling reaction. A brownish-yellow precipitate was formed within the first 1 hour of the reaction which showed the production of insoluble porous polymer network. The coupling of epoxy units in TEPIC with free amines in melamine gives a new alcohol (–OH) functional group in the final COPN-1 product.

The chemical structure of COPN-1 was characterized by solid-state ^{13}C-NMR and FTIR spectroscopy. As shown in Fig. 1a,

the FTIR spectrum of COPN-1 showed strong bands at 1680 and 1453 cm^{-1} arising from the characteristic peaks of the C=N stretching of melamine and the amide carbonyl C=O stretching of isocyanurate. The appearance of the O–H stretching band at 3340 cm^{-1} confirmed the successful Mannich-coupling reaction which resulted to an alcohol unit from the ring-opening of the epoxy group in TEPIC. In addition, the existence of NH stretching band at 3407 cm^{-1} and out of plane bending vibration at 835 cm^{-1} were detected. Finally, aliphatic CH and CN stretching bands at 2907 cm^{-1} and 754 cm^{-1} indicated the formation of COPN-1 network structure respectively.[28]

In the solid-state ^{13}C-NMR spectrum of COPN-1 (Fig. 1b), the peaks in the range of 130–170 ppm are assigned to the aromatic carbons and carbonyl atom of melamine and TEPIC in the COPN-1 structure, respectively. The chemical shift at 132 ppm was the carbonyl of amide unit in TEPIC molecule, and the two chemical shifts at 151 and 142 ppm were the aromatic carbons of melamine which is well consistent with the reported results.[29,30] The other three peaks at 20–70 ppm were the aliphatic peaks of the linker unit between melamine and isocyanide molecules. The chemical shifts of aliphatic carbons next to alcohol (–OH), amine unit of melamine, and nitrogen atom of isocyanide, were 51, 40 and 28 ppm, respectively.[31] The elemental analysis of as-synthesized COPN-1 showed the content of carbon, nitrogen, hydrogen, and the remaining oxygen atoms in Table 1 which were 43.29, 25.19, 5.66, and 25.85 wt%, respectively. These experimental analyses were consistent with the theoretically calculated elemental analysis of the hypothetical COPN-1 structure in Scheme 1. Furthermore, the COPN-1 gave negligible Brunauer–Emmett–Teller (BET) surface area (0.0891 m^2 g^{-1}) and Langmuir surface area (0.1392 m^2 g^{-1}) and showed an average pore size of 7.8533 nm. Therefore, COPN-1 network had low porosity possibly due to linking the aromatic building blocks with aliphatic chains and random orientation of the pores in the network.[32]

In this study, we further aimed to use the COPN-1 network as a template for the *in situ* synthesis of AuNPs. For this purpose, COPN-1 solid was inserted to the HAuCl$_4$ solution with stirring at room temperature to entrap Au(+3) ions inside the polymer network. After a certain time, the mixture was heated to boiling and turned into a red color solution as shown in Fig. 2a (inset). This was the indication for the generation of gold nanoparticles
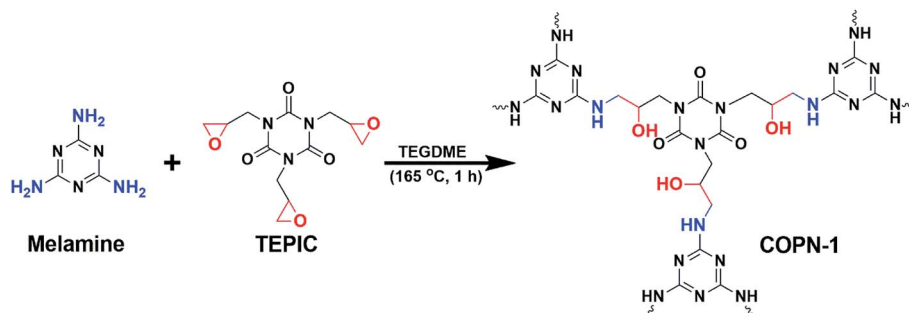
Scheme 1 COPN-1 synthesized *via* reacting tris(2,3-epoxypropyl)isocyanurate with melamine.
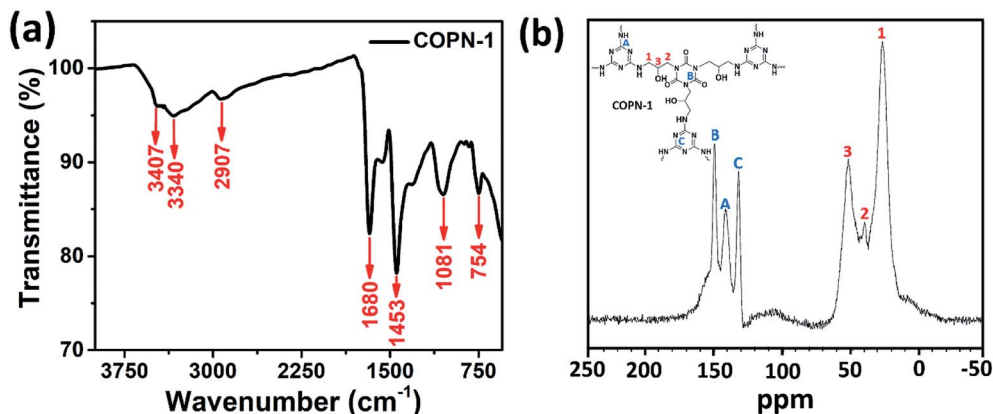
Fig. 1   (a) FTIR and (b) C–NMR spectra of COPN-1.

Table 1   Elemental analysis of COPN-1

Elements (wt%)							
C%		H%		N%		Others%	
Theo.	Exp.	Theo.	Exp.	Theo.	Exp.	Theo.	Exp.
42.55	43.29	5.00	5.66	29.77	25.19	22.66	25.85

(AuNPs) inside the network. After centrifugation, reddish-brown colored precipitate (Au@COPN-1) with yellow-colored supernatant containing Au(+3) ions was obtained. This was an excellent proof for the *in situ* reduction of Au(+3) ions without any reduction of Au(+3) outside the polymer network. In Fig. 2a, the UV-Vis spectrum of the Au@COPN-1 precipitate showed the formation of characteristic surface plasmon band of AuNPs at 545 nm. The sole COPN-1 did not have any peak at 500–700 nm range.

X-ray diffraction (XRD) patterns of the Au@COPN-1 were shown in Fig. 2b. Characteristic patterns of Au@COPN-1 with peaks at 38.33, 44.74, and 64.90° (2θ) correspond to the planes of (111), (200) and (220), respectively.[33] All these diffraction planes were also in good agreement with JCPDS 05-0681. EDX

result (not shown) also confirmed that the COPN-1 structure consisted of Au metal. Furthermore, the crystallite size of AuNPs was calculated as 5.4 nm using the peaks of the (111) and (200) planes based on the Scherrer equation.[34] The XRD spectrum demonstrated the successful *in situ* synthesis of AuNPs inside the COPN-1 network.

Fig. 3a and c showed transmission electron microscopy (TEM) images of Au@COPN-1 with different concentrations of Au(+3) (4.6×10^{-4} mM and 4.6×10^{-3} mM, respectively). These images displayed that AuNPs were only formed inside the COPN-1 network. No AuNPs were remaining outside the matrix, as can be seen by focusing on the single gold nanoparticle highlighted by a red dashed circle at the outer frame of the structure (Fig. 3c). This proved the *in situ* reduction of the Au(+3) within the COPN-1 structure only. The average size and size distribution of the AuNPs, as seen in the inset of Fig. 3a (4.6×10^{-4} mM HAuCl$_4$) and Fig. 3c (4.6×10^{-3} mM HAuCl$_4$), were determined *via* TEM images by using Image J software. It was confirmed that mostly single crystal morphology of AuNPs with increasing sizes was produced as the concentration of Au ions increased. The average sizes of 5.00 ± 3 nm and 35.00 ± 15 nm were calculated. Furthermore, the HR-TEM images given in Fig. 3b and d exhibited the lattice fringe and the interplanar

Fig. 2   (a) UV spectra and (b) XRD Pattern of COPN-1 and Au@COPN-1 (4.6×10^{-3} mM Au).

Fig. 3 (a and c) TEM images of Au@COPN-1 obtained from different concentrations of Au(+3) (4.6×10^{-4} mM and 4.6×10^{-3} mM, respectively) with the corresponding particle size distribution histograms (b and d) The HR-TEM images of Au nanoparticles showing interplanar spacing.

spacing of 0.229 nm and 0.231 nm for the (111) planes of Au(0).[35] The images verified the spherical morphology of nanoparticles.

Fig. 4a showed the UV-Vis absorption spectra of Au@COPN-1 generated by using different concentrations of Au solution. All Au@COPN-1 displayed a characteristic absorption peak in the range of 500–600 nm due to localized surface plasmon resonance of spherical Au nanoparticles.[36]

The amount of $HAuCl_4$ used in the *in situ* reduction process played an important role in determination of the size of Au nanoparticles inside the COPN-1 network. The LSPR peaks of 536, 541, 545, and 550 nm were obtained by using 4.6×10^{-4}, 9.2×10^{-4}, 4.6×10^{-3} and 9.2×10^{-3} mM of $HAuCl_4$, respectively. As indicated in the UV-Vis spectra, there was a clear red shift in LSPR peaks of Au nanoparticles while increasing the concentration of $HAuCl_4$ from 4.6×10^{-4} to 9.2×10^{-3} mM.
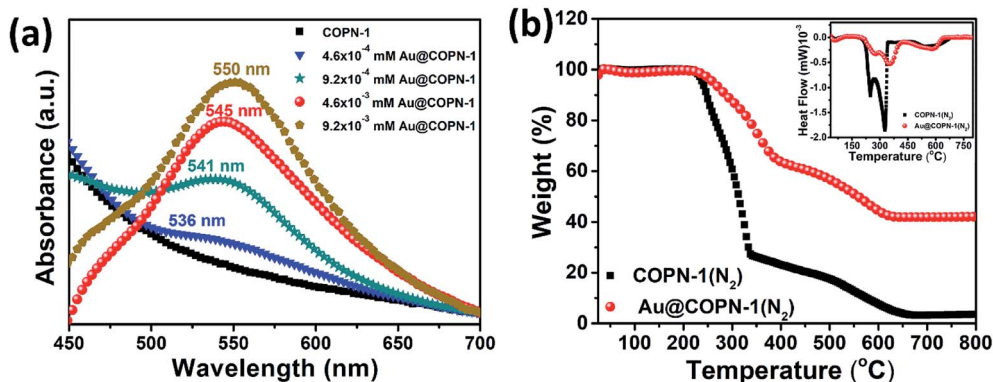

Fig. 4 (a) UV spectra of COPN-1 and Au@COPN-1 at different concentration (4.6×10^{-4}, 9.2×10^{-4}, 4.6×10^{-3} and 9.2×10^{-3} mM Au) (b) TGA thermograms of COPN-1 and Au@COPN-1 (4.6×10^{-3} mM Au) in N_2.

The red-shifting LSPR peaks of Au nanoparticles indicated an increase in the particle size of the Au nanoparticles as previously reported in literature.[37] TEM images (Fig. 3) also confirmed the increase in size with increasing concentration of HAuCl$_4$.

Fig. 4b showed the thermogravimetric analysis (TGA) and differential scanning calorimetry (inset) spectra of both COPN-1 and Au@COPN-1 within the temperature range 25–800 °C carried out under inert atmospheres. According to the DSC results, three endothermic peaks were observed. When the DSC curves and TGA curves were considered together, the endothermic reactions seen in the DSC curves were attributed to the degradation of the COPN-1 polymeric network structure. COPN-1 structure started to degrade at 222 °C and this degradation was completed at about 657 °C. For Au@COPN-1 structure degradation occurred between 239–627 °C. The mass loss observed in COPN-1 and Au@COPN-1 was 94% and 54%, respectively. For the COPN-1 structure, the remaining mass (6%) may be ascribed to carbon-based ash left from the synthesized material. In the Au@COPN-1 structure, the remaining mass (∼46%) was due to the gold used for the synthesis of Au@COPN-1 and the ash remaining from the COPN-1 structure. In the AuCOPN-1 structure, the weight loss between 222 °C and 344 °C was 72% and in the Au@COPN-1 structure, the weight loss between 239 °C and 400 °C was 34%. Furthermore, it was concluded that COPN-1 and Au@COPN-1 structures underwent secondary thermal degradation at temperatures between 493–657 °C and 484–627 °C, respectively. From the TGA graph, it was deduced that Au@COPN-1 structure was more thermally resistant than COPN-1 structure.

Following the characterization of the Au nanoparticles inside the COPN-1 network, we further explored the plausible mechanism for the reduction of HAuCl$_4$ ions to Au atoms by using COPN-1 network. In our synthesis, Au(+3) embedded COPN-1 network in aqueous solution was thermally heated to generate Au nanoparticles in the absence of strong reducing agents like sodium borohydride (NaBH$_4$), which has been commonly used to reduce Au ions inside a matrix. We performed the same reduction of HAuCl$_4$ by using melamine or tris(2,3-epoxypropyl) isocyanurate (TEPIC) instead of COPN-1 network as starting molecules. However, even after prolonged thermal treatments, there was no color change (i.e. the characteristic color of Au nanoparticle) or any precipitate/nanoparticle formation in the reaction solution. This may be ascribed to the lack of thermal decomposition of HAuCl$_4$. Thus, any possible residuals of the starting compounds were not responsible for the reduction of HAuCl$_4$.

During the reduction of HAuCl$_4$ with COPN-1 network, the Au nanoparticles only formed inside the COPN-1 network suggested that the in situ reduction solely underwent through the COPN-1 structure itself. As depicted in Scheme 1, the only structural difference between the starting molecules and COPN-1 matrix was the new hydroxyl (–OH) functional group formed via the Mannich-coupling of epoxy units in TEPIC with free amines in melamine. Having reported in the literature as polyol method, Au nanoparticles could be generated by the reduction

of Au ions with the hydroxyl (–OH) end groups of the polymer chains, for instance, with polyvinylpyrrolidone (PVP).[38] Therefore, in our case, we proposed a polyol-based reduction mechanism shown in Scheme 2.[39] Basically, Au(+3) ions inside the COPN-1 network were reduced to its atomic form Au(0) when the alcohol (–OH) units were oxidized. During the diffusion of HAuCl$_4$ into the COPN-1 matrix, the Au(+3) ions could be chemisorbed onto the amine- or amide-functionalized polymer network which facilitated the entrapment of Au(+3) inside the network leading to the reduction process.[39] With thermal heating, the hydroxyl groups have undergone a redox reaction in which Au(+3) was reduced to zero-valent Au(0). Therefore, the hydroxyl groups in the COPN-1 structure acted as a reductant for Au(+3) ions.

The conversions of aromatic nitro molecules to amines even by using a strong reducing agent, NaBH$_4$, resulted in only about 5% yield due to the high kinetic barrier.[40] Since the discovery of fast conversions of aromatic nitro molecules with high yielding via catalytic Au nanoparticles, there has been a rapid growth in the development of Au catalysts platforms for the reduction of phenolic nitro compounds.[41] These high yielding reduction reactions were catalyzed by AuNPs due to the effective hydrogen transfer from NaBH$_4$ species to nitro units on the reactive surfaces of Au atoms.

In this regard, the catalytic activities of Au@COPN-1 systems were evaluated by the reduction of 4-nitrophenol (4-Nph) to 4-aminophenol (4-Aph) in aqueous solutions. 4-Nph is an essential intermediate for various industries, including pharmaceuticals, corrosion inhibitors, leather darkening, and photographic developers. However acute inhalation and/or ingestion of 4-Nph by humans cause serious health problems.[42] The reduction profiles easily monitored by UV-Vis spectrometry showed a decrease in the absorption peak of 4-Nph at 400 nm and a new peak appearance of 4-Aph at 300 nm. The reduction of 4-Nph only by COPN-1 without using any Au catalyst was also tested. Fig. 5a showed the real-time absorbance spectra for the reduction kinetics of 4-Nph into 4-Aph by COPN-1 which presented a very low conversion within 16 minutes as expected.

After the addition of as-synthesized Au@COPN-1 into the aqueous solution of 4-Nph in the presence of NaBH$_4$, the absorbance peak of 4-Nph at 400 nm started to decrease with a new peak appearance at 300 nm, which revealed the generation of 4-Aph as shown in Fig. 5b. As the reaction proceeded to 16 minutes, the absorbance peak of 4-Nph at 400 nm almost disappeared along with a clear ascent in the peak of 4-Aph at 300 nm. Visually, the yellow color of aqueous reaction solution containing 4-Nph completely disappeared within 16 minutes. Therefore, it can be concluded that the in situ synthesis of AuNPs inside the COPN-1 matrix is a promising catalyst platform for the reduction reactions of aromatic nitro compounds. This investigation demonstrated that the prepared catalyst system was able to degrade dye pollutants and showed promising activity against one of the most common persistent organic pollutants which causes toxicity in industrial and agricultural wastewater.

As shown in Fig. 5c, the kinetics of the reduction reaction of 4-Nph to 4-Aph was explored. To further understand the

Scheme 2 Proposed mechanism for $HAuCl_4$ reduction with COPN-1 in water.

photocatalytic activity of the prepared samples, the kinetic analysis of 4-Nph reduction was investigated. It is generally assumed that the decomposition reaction kinetics can be described with a pseudo-first-order kinetics model. Here, the samples exhibited a linear behavior and the reaction rate constants (k) were estimated from the slope of the plots presented in Fig. 5d. In 4-Nph reduction, Au@COPN-1 catalyst showed much higher activity compared to the $HAuCl_4 \cdot 3H_2O$ and COPN-1 with a rate constant of 0.191 min^{-1}. For the $HAuCl_4 \cdot 3H_2O$ and COPN-1 samples, k was obtained as 0.148 and 0.04 min^{-1}, respectively. However, the k value of the Au@COPN-1 sample was calculated as almost 28% higher than that of $HAuCl_4$. The higher reaction kinetics of Au@COPN-1 than $HAuCl_4 \cdot 3H_2O$ emphasizes the use of supported nanoparticles to heterogeneously catalyze organic transformation reactions.[19]

Furthermore, the Au@COPN-1 has also shown notable recyclability for more than 5 catalytic cycles giving yields over 94% in about 16 min (Fig. 6a). It is noteworthy that the non-aggregation of nanoparticles in the reused catalyst further affirmed the stability of the Au@COPN-1 catalytic system. Thus, it can be stated that the prominent catalytic activity of Au@COPN-1 might be due to the highly stable two-dimensional support of COPN-1 which holds the loaded nanoparticles to a high extent.[19]

The biocompatibility of Au@COPN-1 was studied by using new biosensor technology, the xCELLigence real-time cell analysis system. To gather more accurate information compared to commonly used conventional endpoint cytotoxicity assays (i.e. MTT), the effect of Au@COPN-1 on viability, adhesion and proliferation of L929 fibroblast cells was monitored in real-time for about 10 days by RTCA DP instrument. In

Fig. 5 Catalytic reduction of 4-nitrophenol by using $NaBH_4$, (a) COPN-1, (b) with Au@COPN-1 (4.6×10^{-3} mM Au), (c) kinetics of reduction process of 4-Nph solution (4-Aph formation) and (d) fitted data of the pseudo-first-order kinetics (Au@COPN-1, $HAuCl_4 \cdot 3H_2O$, and COPN-1).

Fig. 6 (a) Recycling experiment of Au@COPN-1 for the conversion of 4-Nph during 5 cycles of reaction and (b) real-time cell analysis results: effect of Au@COPN-1 treatments on L929 cell line proliferation.

this dynamic system, kinetic responses were evaluated to understand the action mechanism of Au@COPN-1 by processing valuable information about cell growth and cellular status changes upon Au@COPN-1 exposure. For analysis, impedance values were calculated as the normalized cell index (the CI from each time point was normalized to the maximum CI attained for the control cell lines at the time zero of the Au@COPN-1 treatment, here normalization time is 19:01:40). According to the cytological profile of L929 cells, incubation with higher doses of Au@COPN-1 (125, 250 and 500 μg mL^{-1}) caused an antimitotic effect (*i.e.* cells remain in a mitotic arrest state) whereas lower dose treatment (62.5 μg mL^{-1}) caused no cytotoxicity (Fig. 6b). Additionally, the IC50 value of Au@COPN-1 was 59.5 μg mL^{-1} for L929 cells. Thus, the cellular effects of Au@COPN-1 shown here may help to design future biomedical applications meticulously.

4. Conclusion

In summary, we have accomplished the *in situ* synthesis of AuNPs inside the COPN-1 matrix without using any reducing agent. We have shown that novel Au@COPN-1 can be used to facilitate the reduction of environmentally toxic aromatic nitro compounds. Herein, the catalytic activity of this new hybrid material showed a successful reduction of 4-nitrophenol with higher performance compared to HAuCl$_4$·3H$_2$O and COPN-1 alone. The *k* value of the Au@COPN-1 sample was calculated as almost 28% higher than that of HAuCl$_4$·3H$_2$O. Furthermore, the catalyst had notable recyclability for more than 5 catalytic cycles giving yields over 94% in 16 min. In addition, the amount of HAuCl$_4$ used in the *in situ* reduction process affected the size of the Au nanoparticles assembled which may be purposive for different applications. The real-time cell analysis results specified the dose-dependent effects of Au@COPN-1 on living cells continuously, valuable data to be used in designing future biomedical applications.

Conflicts of interest

There are no conflicts to declare.

References

1 J. Liu, Y. Fu, X. Fu, Y. Li, D. Liang, Y. Song, C. Pan, G. Yu and X. Xiao, *RSC Adv.*, 2016, **6**, 20834–20842.
2 B. S. Takale, M. Bao and Y. Yamamoto, *Org. Biomol. Chem.*, 2014, **12**, 2005–2027.
3 D. Qu, F. Liu, J. Yu, W. Xie, Q. Xu, X. Li and Y. Huang, *Appl. Phys. Lett.*, 2011, **98**, 113119.
4 M.-C. Daniel and D. Astruc, *Chem. Rev.*, 2004, **104**, 293–346.
5 R. Subair, B. P. Tripathi, P. Formanek, F. Simon, P. Uhlmann and M. Stamm, *Chem. Eng. J.*, 2016, **295**, 358–369.
6 J. Kim, K. R. Kim, Y. Hong, S. Choi, C. T. Yavuz, J. W. Kim and Y. S. Nam, *ACS Appl. Mater. Interfaces*, 2019, **11**(24), 21915–21925.
7 S.-Y. Ding, J. Gao, Q. Wang, Y. Zhang, W.-G. Song, C.-Y. Su and W. Wang, *J. Am. Chem. Soc.*, 2011, **133**, 19816–19822.
8 P. Zhang, Z. Weng, J. Guo and C. Wang, *Chem. Mater.*, 2011, **23**, 5243–5249.
9 Y. Zhou, Z. Xiang, D. Cao and C.-J. Liu, *Chem. Commun.*, 2013, **49**, 5633–5635.
10 S. Subramanian, J. Park, J. Byun, Y. Jung and C. T. Yavuz, *ACS Appl. Mater. Interfaces*, 2018, **10**, 9478–9484.
11 W. Wang, J. Gu, W. Hua, X. Jia and K. Xi, *Chem. Commun.*, 2014, **50**, 8889–8891.
12 A. Zinchenko, Y. Miwa, L. I. Lopatina, V. G. Sergeyev and S. Murata, *ACS Appl. Mater. Interfaces*, 2014, **6**, 3226–3232.
13 A. P. Cote, A. I. Benin, N. W. Ockwig, M. O'keeffe, A. J. Matzger and O. M. Yaghi, *science*, 2005, **310**, 1166–1170.

14 K. Datta, B. S. Reddy, K. Ariga and A. Vinu, *Angew. Chem., Int. Ed.*, 2010, **49**, 5961–5965.

15 R. Ullah, M. Atilhan, B. Anaya, S. Al-Muhtaseb, S. Aparicio, H. Patel, D. Thirion and C. T. Yavuz, *ACS Appl. Mater. Interfaces*, 2016, **8**, 20772–20785.

16 Y. Zhang and S. N. Riduan, *Chem. Soc. Rev.*, 2012, **41**, 2083–2094.

17 Y. Xu, S. Jin, H. Xu, A. Nagai and D. Jiang, *Chem. Soc. Rev.*, 2013, **42**, 8012–8031.

18 S.-Y. Ding and W. Wang, *Chem. Soc. Rev.*, 2013, **42**, 548–568.

19 P. Pachfule, S. Kandambeth, D. D. Díaz and R. Banerjee, *Chem. Commun.*, 2014, **50**, 3169–3172.

20 J. García-Serrano, U. Pal, A. M. Herrera, P. Salas and C. Angeles-Chavez, *Chem. Mater.*, 2008, **20**, 5146–5153.

21 C. G. Wilson, P. N. Sisco, E. C. Goldsmith and C. J. Murphy, *J. Mater. Chem.*, 2009, **19**, 6332–6340.

22 K. Lee, H. Lee, K. H. Bae and T. G. Park, *Biomaterials*, 2010, **31**, 6530–6536.

23 D. Wei, Y. Ye, X. Jia, C. Yuan and W. Qian, *Carbohydr. Res.*, 2010, **345**, 74–81.

24 D. Wei, W. Qian, D. Wu, Y. Xia and X. Liu, *J. Nanosci. Nanotechnol.*, 2009, **9**, 2566–2573.

25 M. a. J. Hortigüela, I. Aranaz, M. a. C. Gutiérrez, M. L. Ferrer and F. del Monte, *Biomacromolecules*, 2010, **12**, 179–186.

26 A. Goyal, A. Kumar, P. K. Patra, S. Mahendra, S. Tabatabaei, P. J. Alvarez, G. John and P. M. Ajayan, *Macromol. Rapid Commun.*, 2009, **30**, 1116–1122.

27 J. Xu, J. Hu, B. Quan and Z. Wei, *Macromol. Rapid Commun.*, 2009, **30**, 936–940.

28 R. A. Chowdhury, M. V. Hosur, M. Nuruddin, A. Tcherbi-Narteh, A. Kumar, V. Boddu and S. Jeelani, *J. Mater. Res. Technol.*, 2015, **4**, 33–43.

29 T. Kotaki, N. Nishimura, M. Ozawa, A. Fujimori, H. Muraoka, S. Ogawa, T. Korenaga, E. Suzuki, Y. Oishi and Y. Shibasaki, *Polym. Chem.*, 2016, **7**, 1297–1308.

30 D. W. Lachenmeier, E. Humpfer, F. Fang, B. Schütz, P. Dvortsak, C. Sproll and M. Spraul, *J. Agric. Food Chem.*, 2009, **57**, 7194–7199.

31 M. Coquelle, S. Duquesne, M. Casetta, J. Sun, S. Zhang and S. Bourbigot, *Polym. Degrad. Stab.*, 2014, **106**, 150–157.

32 P. J. Waller, F. Gándara and O. M. Yaghi, *Acc. Chem. Res.*, 2015, **48**, 3053–3063.

33 C. Krishnaraj, P. Muthukumaran, R. Ramachandran, M. Balakumaran and P. Kalaichelvan, *Biotechnol. Rep.*, 2014, **4**, 42–49.

34 A. Patterson, *Phys. Rev.*, 1939, **56**, 978.

35 T. J. Macdonald, K. Wu, S. K. Sehmi, S. Noimark, W. J. Peveler, H. Du Toit, N. H. Voelcker, E. Allan, A. J. MacRobert and A. Gavriilidis, *Sci. Rep.*, 2016, **6**, 39272.

36 P. Wu, P. Bai, Z. Lei, K. P. Loh and X. Zhao, *Microporous Mesoporous Mater.*, 2011, **141**, 222–230.

37 J. Zhao, X. Zhang, C. R. Yonzon, A. J. Haes and R. P. Van Duyne, *Nanomedicine*, 2006, **1**, 219–228.

38 I. Washio, Y. Xiong, Y. Yin and Y. Xia, *Adv. Mater.*, 2006, **18**, 1745–1749.

39 M. S. Yavuz, W. Li and Y. Xia, *Chem.–Eur. J.*, 2009, **15**, 13181–13187.

40 Z. D. Pozun, S. E. Rodenbusch, E. Keller, K. Tran, W. Tang, K. J. Stevenson and G. Henkelman, *J. Phys. Chem. C*, 2013, **117**, 7598–7604.

41 B. Gole, U. Sanyal and P. S. Mukherjee, *Chem. Commun.*, 2015, **51**, 4872–4875.

42 P. Mulchandani, C. M. Hangarter, Y. Lei, W. Chen and A. Mulchandani, *Biosens. Bioelectron.*, 2005, **21**, 523–527.